Supporting Information for

Elevated dust depositions in West Asia linked to ocean-atmosphere shifts during North Atlantic cold events

Reza Safaierad [a], Mahyar Mohtadi [b*], Bernd Zolitschka [c], Yusuke Yokoyama [d], Christoph Vogt [e], Enno Schefuß [b]

[a] Department of Physical Geography, University of Tehran, 14155-6465 Tehran, Iran; [b] MARUM-Center for Marine Environmental Sciences, University of Bremen, 28359 Bremen, Germany; [c] Institute of Geography (GEOPOLAR), University of Bremen, 28359 Bremen, Germany; [d] Atmosphere and Ocean Research Institute (AORI) and Department of Earth and Planetary Sciences, University of Tokyo, Tokyo 113-0033, Japan; [e] Department of Geoscience, University of Bremen, 28359 Bremen, Germany

Site and sampling

Konar Sandal peat bog (KSB) with an area of 20 ha is located approximately 20 km south of the city of Jiroft in Kerman Province, SE Iran (Fig. 1B) and 2 km west of the 390 km-long Halil River (Halil Rud in Persian). This river originates from the Kerman Massif in the northwest with an elevation of 3300 m a.s.l. and terminates into the Jazmurian Playa in the south. At present, KSB is not an active peat bog and the morphology of the surrounding environment testifies the lack of any fluvial input. However, the proximity to the Halil River as well as the alluvial fans developed at the foothills around the KSB indicate sediment transport via Halil River flooding and surface runoff activities under less arid conditions in the past. Based on the nearest meteorological station (Jiroft), mean annual precipitation (1990-2017) is 177 mm of which >80% occurs from December to March. February with a

mean precipitation of 47 mm and July with 1 mm are the wettest and driest months, respectively. The mean annual temperature is 25.6 °C and January with 13.2 °C and July with 36.4 °C are the coldest and warmest months, respectively. According to Djamali*, et al.* (1), Jiroft is located in a tropical desert-like bioclimatic region characterized by extremely hot, dry summers and moderate temperatures in winter. SE Iran is mainly influenced by the mid-latitude westerlies at present and only occasionally receives rainfall from the ISM (2) (Fig. S2).

In May 2017, we recovered a 7.63 m-long sediment sequence from KSB with a Russian peat corer (Lat. 28° 32′ 02″ N, Lon. 57° 46′ 53″ E, 570 m a.s.l.). The core sections are 0.5 m-long with a diameter of 5 cm. The core segments were wrapped in plastic and placed in PVC core liners. In order to prevent cores from drying and contamination by either external contaminants or algal growth, the cores were stored in a fridge (4 °C) at the University of Tehran for three weeks until they were firmly packed and transferred to Germany with airplane. Samples were then immediately stored at 4 °C in the core repository at MARUM-Center for Marine and Environmental Sciences, University of Bremen. Here we report on the section between 169 and 763 cm sediment depth, spanning the time period 19–6.85 cal. ka BP.

Materials and Methods

Elemental analysis by X-Ray Fluorescence core scanning

In order to evaluate downcore changes in element composition, XRF core scanning was processed using the AVAATECH XRF core scanner at MARUM, University of Bremen. Before scanning, the sediment surfaces were covered with a 4 µm-thin SPEXCerti Prep Ultralene foil to avoid contamination of the XRF measuring unit and desiccation of the sediment. XRF Core Scanner data were measured every 1 cm downcore across a 12 mm^2

area with a slit size of 10 mm using three different voltages of 50, 30 and 10 kV with 0.75, 0.75 and 0.2 mA, and analyzing times of 25, 20 and 15 s, respectively. The reported data have been acquired by a Canberra X-PIPS Silicon Drift Detector (SDD; Model SXD 15C-150-500) with 150 eV X-ray resolution, a Canberra Digital Spectrum Analyzer DAS 1000, and an Oxford Instruments 50W XTF5011 X-ray tube with a rhodium (Rh) target. Raw spectra were processed by the Iterative Least square software (WIN AXIL) package from Canberra Eurisys. The abundance of elements is reported as intensity of each element in counts per second (counts S^{-1}). XRF core scanning as a fast and non-destructive technique is widely used in paleoenvironmental studies in order to analyze the elemental composition of sediment cores (3), which is particularly useful in studying past aeolian activities. Different elements behave differently in terms of mobility and redox-sensitivity against hydrochemical processes. These differences are keys to infer mechanisms at play with sediment transportation and environmental conditions during which sediments have been deposited as well as post-depositional modifications. As our site is in proximity to large deserts, it is highly susceptible to record past aeolian activities. Thus, we measured elemental compositions of our sediment core in order to detect sedimentary transport mechanisms.

Radiocarbon dating

Based on variations in the abundances of lithogenic elements measured by XRF core scanning, seven samples were selected for radiocarbon dating. Bulk samples were sieved through a 250 µm screen. Seeds and micro-charcoal particles >250 µm were picked and submitted for ^{14}C dating to the AMS Radiocarbon Dating Laboratory of the University of Tokyo, Japan. Radiocarbon dates (Table S1) were calibrated using the Northern Hemisphere IntCal13 calibration dataset (4). The age model was constructed using the CLAM package, version 2.2 (5), in the open source software “R” (6). CLAM creates a “best

fit" curve based on the weighted average of 1000 iterations of age probability distributions. The 95% confidence intervals are based on a 2σ range of average iterations. All ages reported are presented as calibrated thousand years before AD 1950 (cal. ka BP).

Mineralogical analysis by X-Ray Diffraction (XRD).

Twelve samples about 1 g of weight were selected from sections with high and low Ti content. Samples were dried at 50 °C for 48 hours. The dried samples were ground and homogenized using mortar and pestle. XRD analyses were carried out at the Central Laboratory for Crystallography and Applied Material Sciences, ZEKAM, Dept. of Geosciences, University of Bremen. The X-ray diffractograms have been measured on a Philips X'Pert Pro multipurpose diffractometer equipped with a Cu-tube (k" 1.541, 45 kV, 40 mA), a fixed divergence slit of ¼°, a 16 sample changer, a secondary Ni-Filter, and the X'Celerator detector system. Measurements were performed as a continuous scan from 3–85° 2θ, with a calculated step size of 0.016° 2θ (calculated time per step was 100 s). Minerals were identified with the Philips/Panalytical software X'Pert HighScore™, which can also give a semi-quantitative value for each identified mineral on the basis of Relative Intensity Ratio (R.I.R)-values. The R.I.R.-values are calculated as the ratio between the intensity of the most intense reflex of a specific mineral phase and the intensity of the most intense reflex of pure corundum (I/Ic) referring to as the "matrix-flushing method" after Chung (7).

Grain-size analysis

A number of 29 samples were picked from sections with high and low Ti content from the 737-195 cm depth interval of the KSB sediment record. Subsamples of 0,3 g were treated with H_2O_2 to remove organic matter, first overnight and at room temperature and then for two hours at 105 °C. Prior to analysis with a LS 200 Laser Diffraction Particle Size Analyzer (Beckman Coulter) equipped with a variable speed module at the GEOPOLAR lab

(Institute of Geography, University of Bremen), samples were dispersed with 20 ml of Calgon and agitated with a shaking device. Samples were transferred to the analyzing unit through a 2 mm sieve and measured at least four times for 60 s with sonification. From at least three individual measurements with a stable grainsize distribution arithmetic means were calculated. Finally, statistical parameters of grainsize distributions were obtained with the software package GRADISTAT for the analysis of unconsolidated sediments (8).

Organic carbon analysis

Sixty samples from the depth interval 761-176 cm of the KSB sediment core were subsampled with a mean spatial resolution of 9.4 cm, dried in an oven at 50 °C for 48 hours and ground and homogenized using mortar and pestle. Then, samples were weighed into silver capsules and pretreated with 3% and 20% HCl overnight at a temperature of 80 °C to remove carbonates. Finally, samples were analyzed with a Euro-EA Elemental Analyzer at the GEOPOLAR lab (Institute of Geography, University of Bremen) providing weight percentages of total organic carbon (TOC).

Chronology and lithology

The age model based on seven calibrated ^{14}C dates (Table S1) is illustrated in Fig. S3. According to the age-depth model, the KSB core covers the period 19–0.6 cal. ka BP. The consistency between ^{14}C dates obtained from charcoal particles and seeds at a depth of 324 cm indicates that charcoal particles are derived from *in situ* burning of local vegetation and thus deliver accurate ^{14}C ages. The lithology for the last deglaciation (below 550 cm) alternates between sandy mud (light colored: 550-583 cm and 652-669 cm, and dark colored: 670-738 cm), and gyttja (584-651 cm and 739-763 cm), while the lithology of the Early Holocene (550-169 cm) is composed of gyttja - apart from muddy gyttja between 202-230 cm (Fig. S3). The sedimentation rate at the base of the core (763-550 cm) is low and varies between 0.22 and 0.35 mm yr^{-1} from 19–11.7 cal. ka BP. From 11.7–10.3 cal.

ka BP the sedimentation rate increases to 1.5 mm yr^{-1} (550-324 cm). This change is accompanied with a change in lithology from sandy mud to gyttja. Sedimentation rate decreases to 0.55 mm yr^{-1} between 10.3-8.8 cal. ka BP and to 0.38 mm yr^{-1} between 8.8-6.8 cal. ka BP.

References

1. Djamali M*, et al.* (2011) Application of the global bioclimatic classification to Iran: implications for understanding the modern vegetation and biogeography. *Ecologia mediterranea* 37(1):91-114.
2. Raziei T, Daryabari J, Bordi I, & Pereira LS (2014) Spatial patterns and temporal trends of precipitation in Iran. *Theoretical and applied climatology* 115(3-4):531-540.
3. Croudace IW, Löwemark L, Tjallingii R, & Zolitschka B (2019) Current perspectives on the capabilities of high resolution XRF core scanners. *Quaternary international* 514:5-15.
4. Reimer PJ*, et al.* (2013) IntCal13 and Marine13 radiocarbon age calibration curves 0–50,000 years cal BP. *Radiocarbon* 55(4):1869-1887.
5. Blaauw M (2010) Methods and code for 'classical'age-modelling of radiocarbon sequences. *quaternary geochronology* 5(5):512-518.
6. R Development Core Team R (2013) R: A language and environment for statistical computing.
7. Chung FH (1974) Quantitative interpretation of X-ray diffraction patterns of mixtures. I. Matrix-flushing method for quantitative multicomponent analysis. *Journal of Applied Crystallography* 7(6):519-525.

8. Blott SJ & Pye K (2001) GRADISTAT: a grain size distribution and statistics package for the analysis of unconsolidated sediments. *Earth surface processes and Landforms* 26(11):1237-1248.
9. Folk RL (1980) *Petrology of sedimentary rocks* (Hemphill Publishing Company).
10. Pourmand A, Marcantonio F, & Schulz H (2004) Variations in productivity and eolian fluxes in the northeastern Arabian Sea during the past 110 ka. *Earth and Planetary Science Letters* 221(1-4):39-54.
11. Vaezi A*, et al.* (2019) A Late Pleistocene-Holocene multi-proxy record of climate variability in the Jazmurian playa, southeastern Iran. *Palaeogeography, palaeoclimatology, palaeoecology* 514:754-767.
12. Sharifi A*, et al.* (2018) Early-Holocene greening of the Afro-Asian dust belt changed sources of mineral dust in West Asia. *Earth and Planetary Science Letters* 481:30-40.

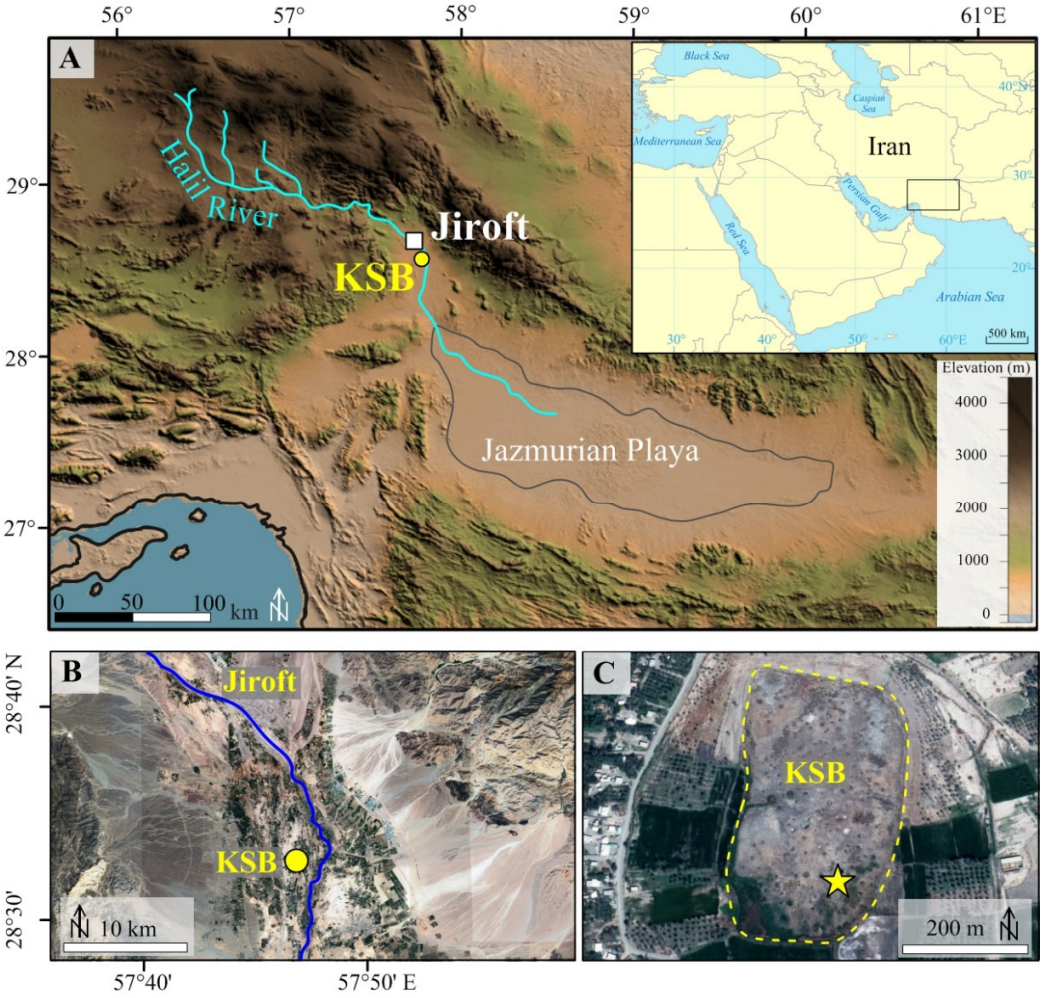

Fig. S1. Location of the study area. (A) Topographic map of the study area in SE Iran. The box in the inset map indicates the position of the study area in West Asia. (B) Satellite image of KSB and surrounding mountains. Blue line indicates the Halil River (date of image December 2016). (C) Satellite image of KSB. Yellow star denotes the coring position and the yellow dashed line marks the area of KSB (date of the image March 23, 2018).

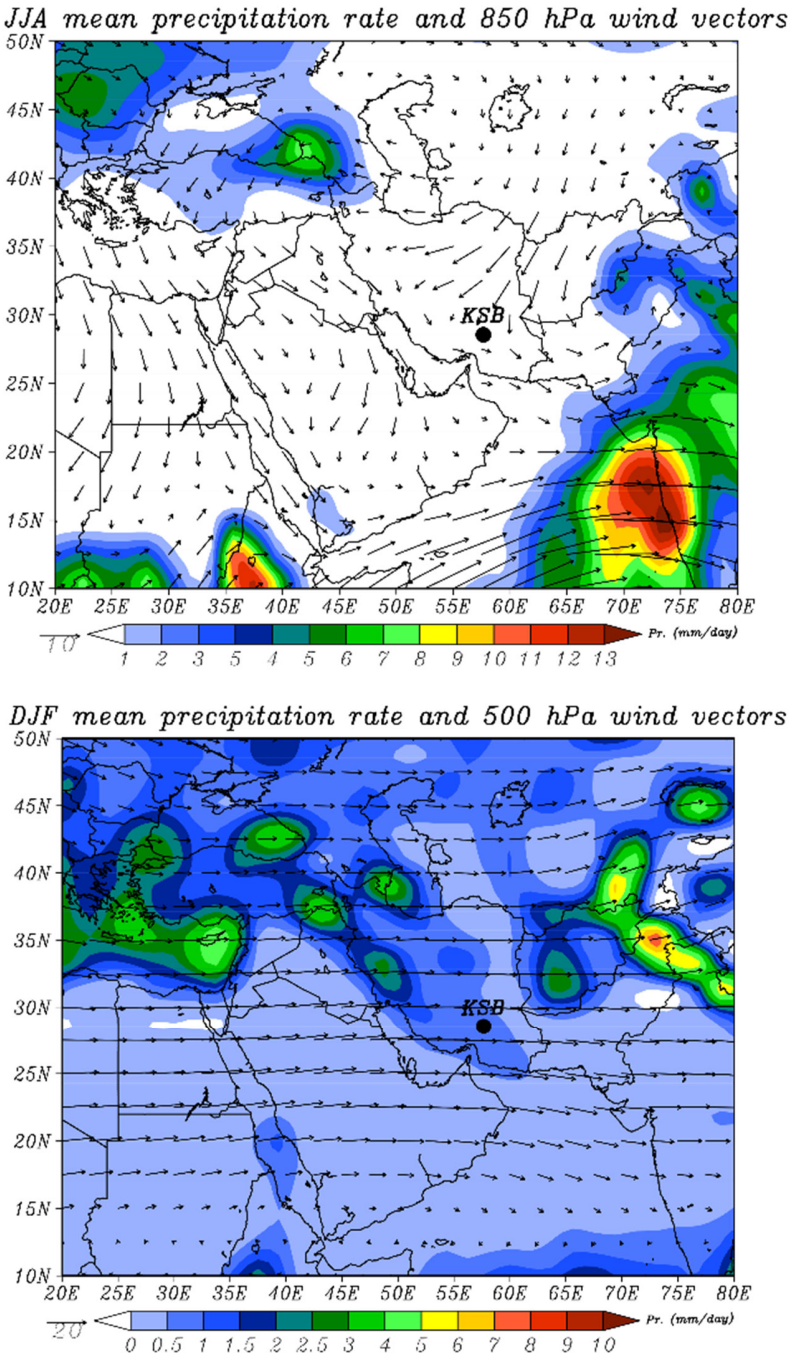

Fig.S2. NCEP seasonal long-term mean precipitation rate (mm/day, shaded) and wind vectors (850 hPa for summer and 500 hPa for winter) over West Asia for summer (JJA: June-July-August, top panel) and winter (DJF: December-January-February, bottom panel). Black dot labeled as KSB represents the location of our site.

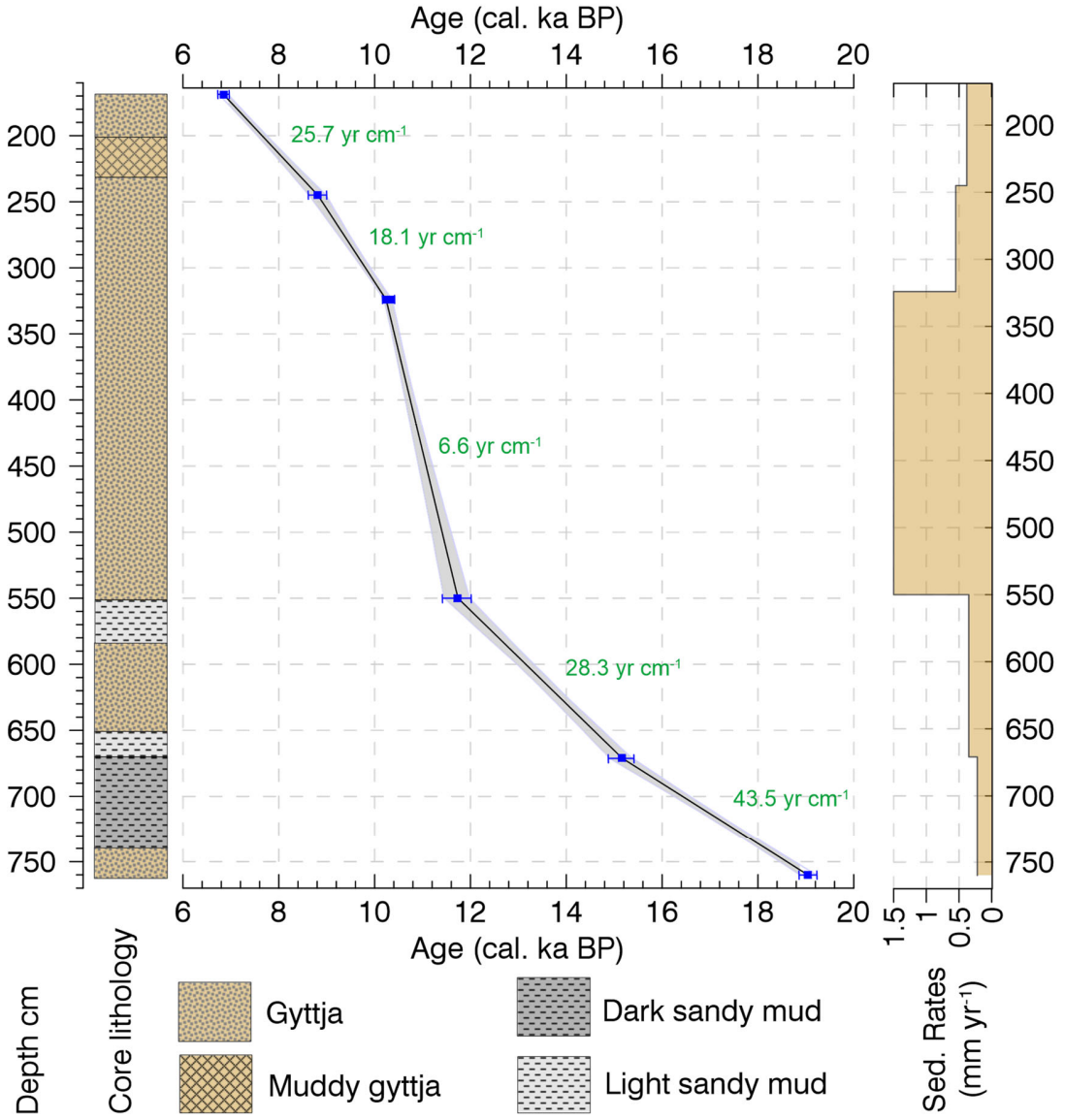

Fig. S3. Age-depth model and lithology of the Konar Sandal peat bog, SE Iran. The gray area between the median calibrated ages (blue tie points) indicates the 2σ uncertainty. Sedimentation rates (Sed. Rates) between radiocarbon dates are shown on the right-hand side. Average temporal resolution (yr cm^{-1}) for each segment of the age model is shown in green along the age-depth curve.

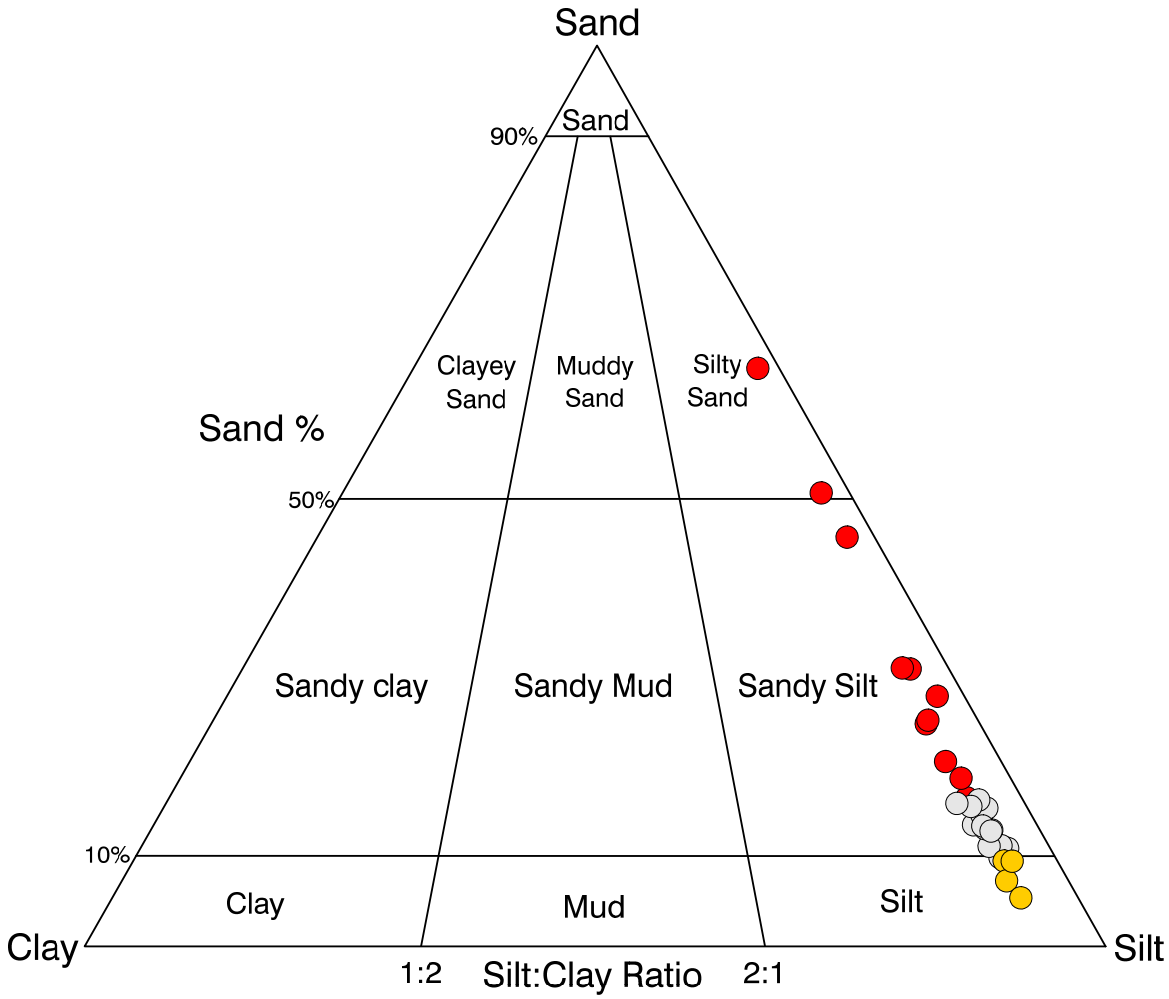

Fig. S4. Distribution of grain-size data plotted on the sand-silt-clay ternary diagram (9). Red dots indicate Early Holocene samples, gray dots denote samples of the last deglaciation, and yellow dots correspond to samples between 8.4 and 7.9 cal. ka BP, i.e. for the period of the 8.2-ka event.

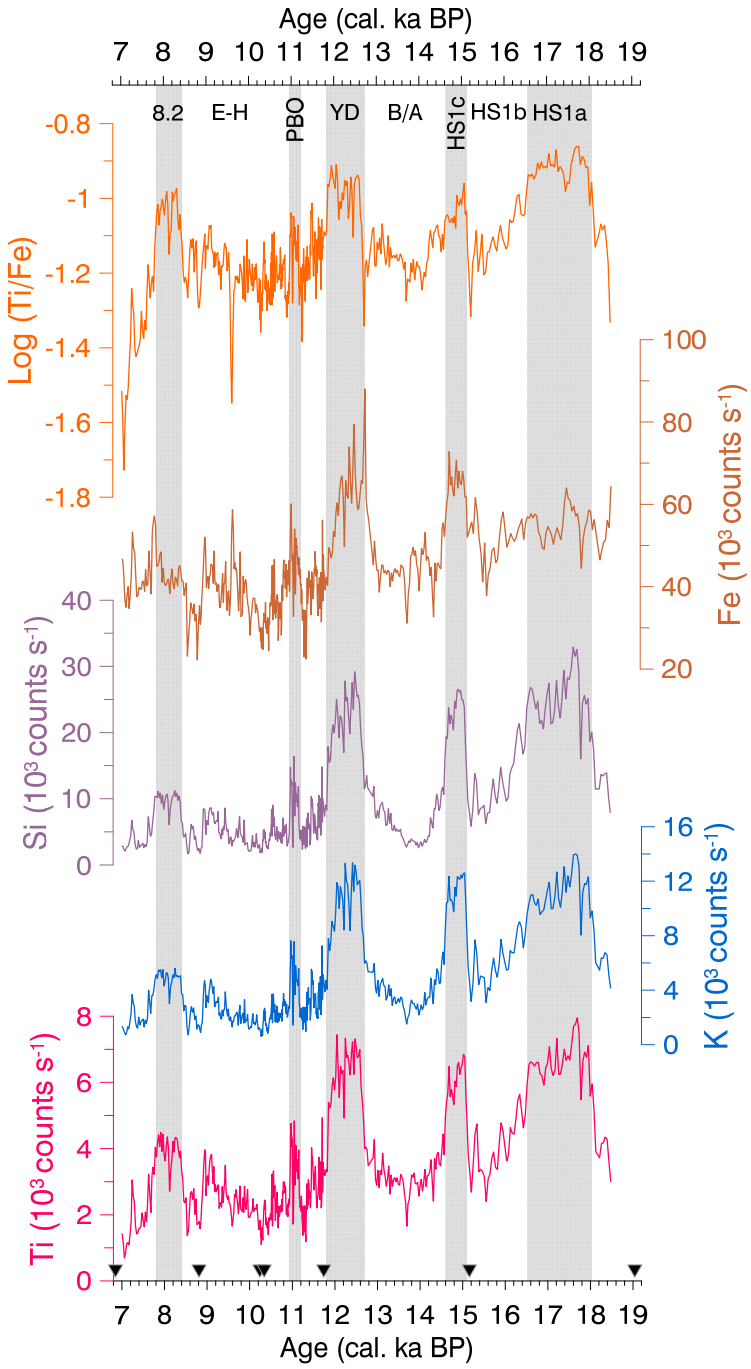

Fig. S5. Downcore elemental abundances for immobile (Ti and Si), mobile (K), and redox-sensitive (Fe) elements along with the Ti/Fe ratio. Gray bands mark peaks of dust input. HS1: Heinrich Stadial 1, B/A: Bølling-Allerød interstadial, YD: Younger Dryas stadial, PBO: Preboreal Oscillation, E-H: Early-Holocene, and 8.2: the 8.2 ka event. Black triangles at the bottom of the figure indicate ^{14}C age control points.

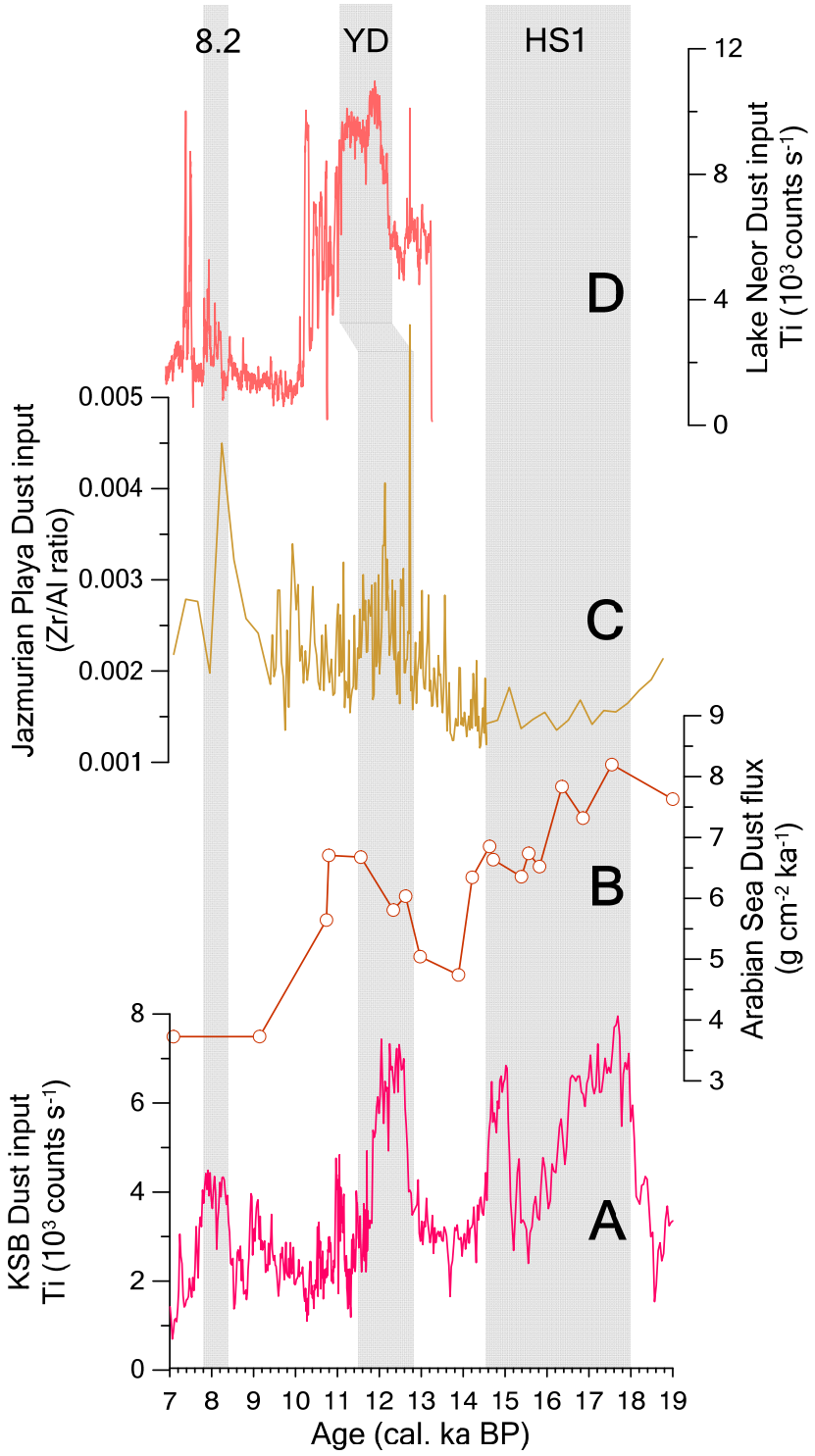

Fig. S6. Comparison of the KSB Ti record from SE Iran (A, this study), as a proxy for dust input in SE Iran with dust records from West Asia. (B) $^{230}Th_{xs}$-normalized dust mass

accumulation rates at core 93KL from the Arabian Sea (10) as a proxy for dust input into the Arabian Sea. (C) Zr/Al ratio of core Jazmurian Playa (11) as a proxy for dust input in SE Iran. (D) Ti record of Neor sediment core (12) as a proxy for dust input in NW Iran. HS1: Heinrich Stadial 1, YD: Younger Dryas stadial, and 8.2: the 8.2-ka event.

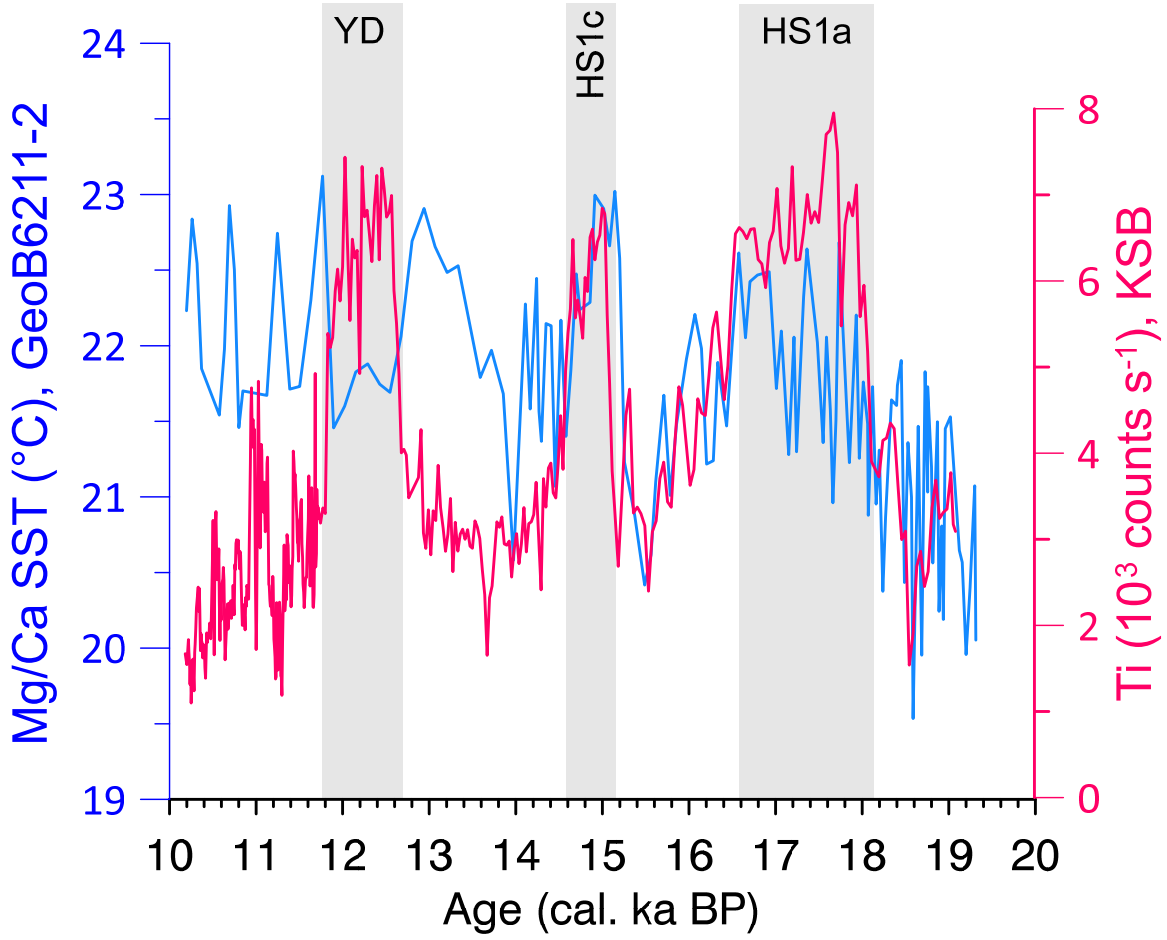

Fig. S7. Comparison of the KSB Ti record from SE Iran (red curve, this study), as a proxy for dust input in SE Iran with Mg/Ca SST variations of core GeoB6211-2 (blue curve) from the western South Atlantic. Note the high correlation during Heinrich Stadial 1 (HS1: Heinrich Stadial 1, YD: Younger Dryas stadial).

Table S1. Radiocarbon dates and calibrated ages with ±2σ probability ranges.

Lab. Code	Depth (cm)	Material dated	^{14}C age (yr BP)	2σ Age-ranges (cal. yr BP)	Calibrated age (cal. yr BP)
YAUT-035402	169	Micro-charcoal	6010 ± 42	6750-6950	6850 ± 55
YAUT-034837	245	Seeds	7950 ± 52	8630-8990	8810 ± 21
YAUT-033205	324	Seeds	9080 ± 43	10220-10260	10240 ± 22
YAUT-033206	324	Micro-charcoal	9170 ± 52	10270-10410	10340 ± 39
YAUT-033209	550	Micro-charcoal	10110 ± 45	11450-11980	11730 ± 106
YAUT-035403	671	Micro-charcoal	12730 ± 65	14900-15380	15160 ± 97
YAUT-033211	760	Micro-charcoal	15790 ± 67	18880-19220	19040 ± 94